Received December 15, 2021, accepted January 9, 2022, date of publication January 14, 2022, date of current version February 3, 2022.

Digital Object Identifier 10.1109/ACCESS.2022.3143537

Electromechanical Coupling Dynamic Characteristics of Differential Speed Regulation System Considering Inverter Harmonics Under Variable Operating Conditions

DIANRUI WANG[1], FUCHUN YANG[1,2], XIAOFENG JIANG[1], SHUAI SHI[1], AND SONGHUA MA[1]

[1]Key Laboratory of High Efficiency and Clean Mechanical Manufacture of MOE, School of Mechanical Engineering, Shandong University, Jinan 250061, China
[2]National Demonstration Center for Experimental Mechanical Engineering Education, Shandong University, Jinan 250061, China

Corresponding author: Fuchun Yang (fuchunyang@sdu.edu.cn)

This work was supported in part by the National Natural Science Foundation of China under Grant 51775309, in part by the China Postdoctoral Science Foundation under Grant 2021M691704, and in part by the Key Technology Research and Development Project of Shandong Province under Grant 2019GGX104013.

ABSTRACT The differential speed regulation system driven by inverters, motors and differential gear trains is a complex electromechanical system that achieves speed regulation and energy savings efficiently and economically. In this paper, the complete drive trains dynamic model of the differential speed regulation system with the inverter power supply-motor-differential gearbox-load is established. The inverter power supply considers constant voltage to frequency ratio control, sinusoidal pulse width modulation and inverter, the motors are modeled based on the equivalent circuit method, and the differential gear trains consider a lateral-torsional model with time-varying meshing stiffness and damping. The dynamic properties of the system are analyzed and compared with the variable frequency drive model considering inverter power supply and the direct drive model using ideal power supply under variable operation conditions. The results show that the variable frequency drive model varies more smoothly in the time domain and contains additional harmonic components in the frequency domain resulting from the coupling of the inverter triangle carrier frequency to the fundamental frequency of the power supply than the direct drive model. It also shows that the variable frequency drive model is a more realistic and rational model than the direct drive model. The complex coupling relationship can be seen in the inverter power supply-motor-differential gearbox-load system, where both inverter harmonics and mechanical meshing force harmonics are found in the dynamic response of the motor's electromagnetic torque, rotor speed; the inverter harmonics are also reflected in the mechanical meshing force harmonics.

INDEX TERMS Electromechanical coupling, inverter, differential gears train, speed regulation, energy saving.

I. INTRODUCTION

Variable speed drive (VSD) is a device that regulates the speed and rotational torque of mechanical equipment. The application of variable speed drives can increase productivity and save energy for pumps, fans, compressors, and other large industrial equipment [1]–[3]. The main forms of variable speed drives used in the industrial sector are hydraulic coupling speed regulation, mechanical speed regulation, and electrical speed regulation. The hydraulic coupling speed regulation is based on the principle of changing the speed difference between the active and driven shafts by changing the amount of oil in the coupling. Mechanical speed regulation mainly refers to the use of belts or gearboxes, both have some disadvantages, such as the use of gearboxes cannot achieve step-less speed regulation, the use of belts can achieve step-less speed regulation, but the accuracy cannot be maintained; most of the industrial power source

The associate editor coordinating the review of this manuscript and approving it for publication was Lei Wang.

for three-phase induction motors, electrical speed regulation methods are generally frequency control. The efficiency and accuracy of variable frequency drives are high, but the cost of the equipment and its maintenance is also expensive, especially when driving high-power motors with variable frequency drives. The differential characteristics of planetary differential gearboxes [4] combined with variable frequency drive energy-saving principle [5], high-power motors drive the gear ring constant speed operation, low-power motors for frequency control indirect drive carrier can achieve low equipment and maintenance costs, high efficiency to achieve differential speed regulation energy saving. With the emphasis on energy saving and consumption reduction, power plants and oil and gas transmission enterprises to the original fixed speed equipment to implement frequency conversion is a major trend [6]–[8].

Nowadays, severe electromechanical coupling effects are often observed in large rotating machines driven by asynchronous motors and controlled by inverters under variable speed drives, generating additional fluctuating drive torque components under transient and steady-state operating conditions [9]. The inverter-generated variable frequency power supply acts directly as an input to the motor, which acts as a power source for the gearbox, while the torque of the gearbox input shaft is also a load on the motor, with the three components interacting with each other. Many scholars have studied the dynamic characteristics of motor-gearbox electromechanical coupling: Khabou [10] established a coupled dynamics model of motor-gear pair-pump and analyzed the dynamic response of the gear pair in terms of vibration displacement, dynamic meshing force and transmission error when the system is in the motor start-up phase and subjected to periodic fluctuating load. Bai [12] established a non-linear dynamics model for a multi-motor gear system and investigated its dynamic characteristics, considering the effects of motor rotational inertia, mounting errors and time-varying meshing stiffness. The above models consider the mechanical and torsional characteristics of the motor but do not consider the electromagnetic effects of the motor, inverter harmonics, and variations in operating conditions. Szolc [9] studied the electromechanical coupling characteristics of an asynchronous motor and rotating machine drive system, and determined the electromagnetic stiffness and damping coefficients of the electromechanical system using the analytical method. Yi [13] established a model of an induction motor based on an equivalent circuit and a dynamics model of a multi-stage gear drive and analyzed the influence of the electromagnetic characteristics of the motor on the natural characteristics and dynamic response of the drive system. Bai [11], [14] considered the effects of magnetic saturation of induction motor and machine slotting, and established the magnetic permeability network model of induction motor, combined with the lumped-parameter model of planetary gear, to analyze the dynamics of the electromechanical coupled system under load saltations and voltage transients. Liu [15] combined the lumped-parametric model of the sun gear and planetary gear with the finite element model of the ring and planetary carrier to propose a hybrid mechanical model to study the dynamic characteristics of the electromechanical coupling under the known dynamic electromagnetic torque excitation of the motor. Shu [16] established a model of the electromechanical coupling dynamics of a multi-source drive system which included the gear system, the load and the drive motors, and investigated the effect of different loads on the synchronization characteristics of the system. The above-mentioned papers modelled the electromechanical coupling between motor and gearbox, but oversimplified the supply voltage at the motor input and did not consider the influence of the inverter.

With the development of variable frequency speed regulation technology, Song-Manguelle [17] found that fluctuations in electromagnetic torque caused by high harmonic voltages generated during the operation of inverters are one of the main causes of failures in mechanical equipment, and pointed out that the frequency of fluctuating torque has a more significant impact on failures than the magnitude of fluctuations. Feese [18] found that excessive vibration and failure of the coupling and motor shaft of the fan system under variable frequency drive was caused by the interaction between the electrical PWM inverter and the mechanical modes. Itoh [19] compared between V/f control and position-sensorless vector control method, showed that V/f control is the best choice for simple variable-speed applications such as fan or pumps and is especially effective in the high-speed range. Lysenko [20] took constant voltage to frequency ratio control into account and simulated a real three-phase inverter-induction motor-centrifugal pump. Han [21] established an electromechanical coupling model in open-loop voltage to frequency control mode and calculated and analyzed the effect of factors such as multi-stage inverters on fatigue life. Song-Manguelle [22] considered pulse-width modulation, inverters, while simplifying a dynamic mechanical load to a variable frequency drive containing harmonics, and investigated the interaction between electrical and mechanical harmonics. The above studies show that inverters have an important influence on the drive system when studying the dynamic characteristics of electromechanical coupling.

In the dynamic characteristics analysis method, most scholars [12]–[22] mainly focus on the dynamics of electromechanical inter-coupling of systems in the steady state, and some scholars also study the dynamic characteristics of electromechanics under transient conditions for some electrical systems with transients [11] or sudden changes in mechanical loads [10], [23]. However, for differential speed regulation systems, it is very basic and common for the variable frequency drive to produce smooth changes in the mechanical load. Therefore, it is necessary to carry out transient analysis of the start-up and speed regulation stages in addition to the study of the steady state characteristics of the differential speed regulation system.

Some of the above-mentioned scholars [10]–[16] have studied the dynamic characteristics of motor-gear system coupling, while others [17]–[22] have analyzed the dynamic characteristics of inverter-motor coupling or inverter-motor-pump coupling. These studies only consider part of the electromechanical drive system and do not provide a complete reflection of the overall coupling dynamic characteristics of the electromechanical coupling system. To solve the above issues, the complete drive trains dynamic model of the differential speed regulation system with the inverter power supply-motor-gearbox-load is established in this paper, which includes the fan-pump load, the differential planetary gear lateral-torsional model, the motor equivalent circuit model, and the inverter model. The differential gear lateral-torsional model considers the time-varying meshing stiffness in generalized angular coordinates and damping, the motor equivalent circuit model considers the voltage equation, the magnetic chain equation, and the electromagnetic torque equation, and the inverter power supply model considers constant voltage to frequency (V/f) ratio control, sine pulse width modulation (SPWM) and inverter harmonics. The dynamics of the differential speed regulation system are investigated in the start-up, steady-state and speed regulation stages.

The rest of the paper is structured as follows: Section 2 presents the differential planetary gear lateral-torsional model and the load model; Section 3 presents the motor equivalent circuit model; Section 4 presents the inverter power supply model; Section 5 investigates the dynamic characteristics and parameter effects of differential speed regulation systems under variable frequency drive and direct drive during start-up, steady-state and speed regulation stages. Finally, Section 6 gives the conclusions and recommendations of the study.

II. MODEL OF THE DIFFERENTIAL PLANETARY DIFFERENTIAL GEAR SYSTEM AND LOAD

This paper investigates the dynamic characteristics of the electromechanical coupling of a differential speed regulation system for fans or pumps, the composition of which is shown in Fig. 1. The power system mainly includes the three-phase power supply and inverter power supply containing V/f control, SPWM and inverter. The motor part consists of a main motor providing the main power and two auxiliary low-power motors for speed regulation in order to balance the forces on the system. The mechanical system is composed of 2K-H type planetary differential gears and fixed shaft gears for the synthesis of power and motion to achieve a certain range of speed regulation. The electrical section is connected as shown in the imaginary line. The main motor does not need to go through the inverter as the auxiliary motor is driven by a variable frequency drive. The mechanical part is connected as shown in a straight line. The main motor drives the ring directly through the connecting shaft, the two auxiliary motors drive the external gears through the connecting shaft and then indirectly drive the carrier through

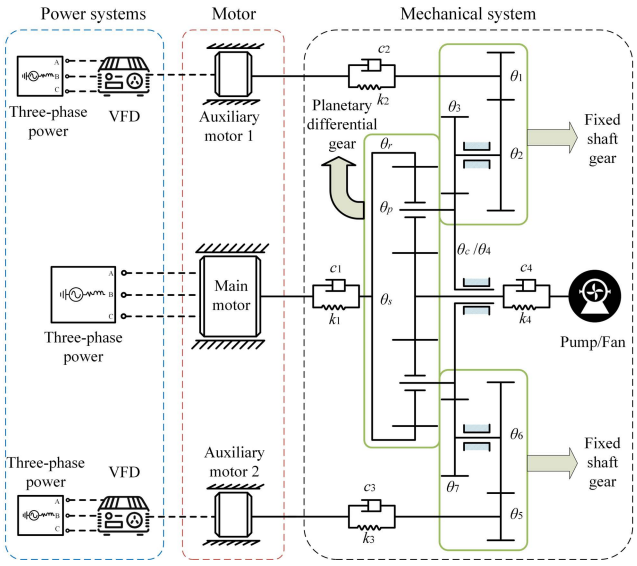

FIGURE 1. Schematic of the differential speed regulation system.

the fixed gears system, the sun gear is connected to the load by a shaft, which acts as an output to increase the speed and reduce the torque. When the system needs speed regulation, the speed of the main motor is kept constant and the speed of the two low-power motors is adjusted synchronously to achieve the final speed regulation requirement at the load side.

Angular displacement is chosen as the generalized coordinate in the dynamical model of the gears system. In this section, the lateral-torsional dynamics of a planetary differential gears system are developed. In Fig. 2, three kinds of coordinate systems are constructed: (1) the static coordinate system $o_i x_i y_i (i = 1, 2, 3, c, 4, 5, 6)$; (2) the moving coordinate system $o_i x_i y_i (i = s, r)$ rotating with the carrier; (3) the moving coordinate system $o_{pi} x_{pi} y_{pi}$ $(i = 1, \ldots, N)$ (N is the number of planetary gears) rotating on the carrier, where the x_{pi}-axis is in the radial direction and the y_{pi}-axis is in the tangential direction. The angular displacement of each gear is measured in the corresponding coordinate system, $[\theta_s, \theta_r, \theta_c, \theta_1, \theta_2, \theta_3, \theta_5, \theta_6, \theta_7, \theta_{p1}, \ldots, \theta_{pN}]$ being the generalized coordinates of the planetary gear system.

In this paper, the equations of motion of the planetary differential system are derived using Newton's laws in the non-inertial system. In the planetary gear section, as the sun gear, planetary gears and ring translation vibrations are all associated with the rotation of the carrier, the translational vibration acceleration of the planetary gears' components should contain not only the translational acceleration but also the centripetal accelerations, the Coriolis accelerations and the tangential accelerations of the carrier. For example, the position of the sun gear is $r_s = x_s i + y_s j$, and the translational acceleration of the sun gear is $\ddot{r}_s = (\ddot{x}_s - 2\dot{\theta}_c \dot{y}_s - \dot{\theta}_c^2 x_s - \ddot{\theta}_c y_s) i + (\ddot{y}_s + 2\dot{\theta}_c \dot{x}_s - \dot{\theta}_c^2 y_s + \ddot{\theta}_c x_s) j$. In the planetary differential system, since the speed of the carrier is not very high, the Coriolis acceleration $2\dot{\theta}_c \dot{y}_s$, $2\dot{\theta}_c \dot{x}_s$ and the centripetal

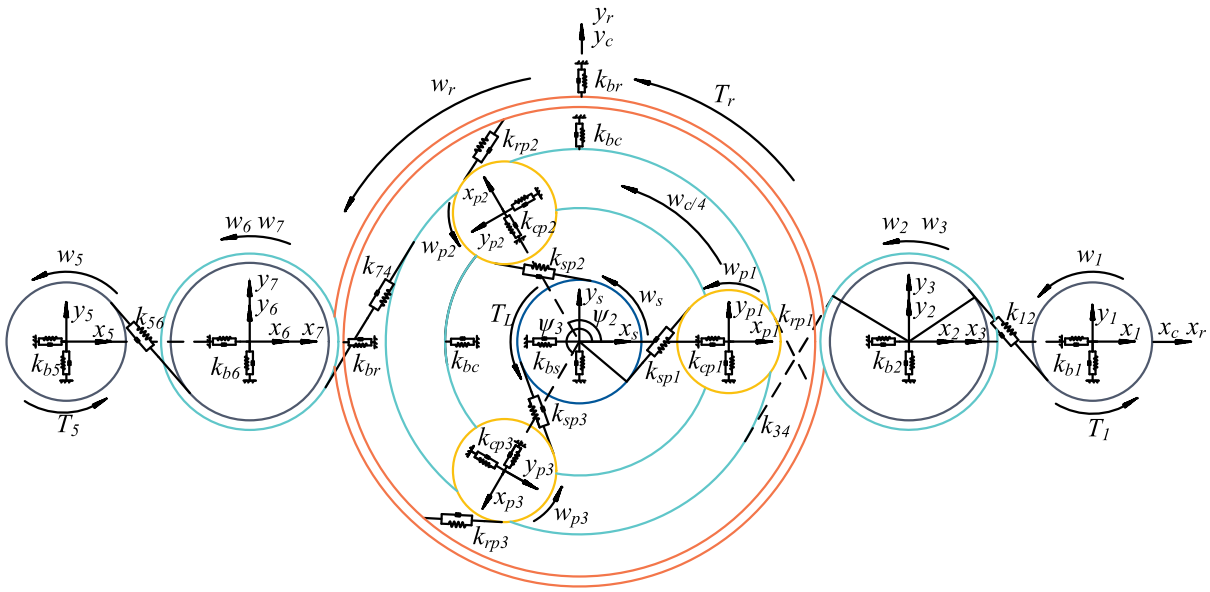

FIGURE 2. Dynamic model of the differential gear train.

acceleration $\dot{\theta}_c^2 x_s, \dot{\theta}_c^2 y_s$ can be neglected. Considering that there is a variable speed process in the differential system, the tangential acceleration of the carrier $\ddot{\theta}_c x_s, \ddot{\theta}_c y_s$ is taken into account, so the translational vibration acceleration of the sun gear is $\ddot{r}_s = (\ddot{x}_s - \ddot{\theta}_c y_s)i + (\ddot{y}_s + \ddot{\theta}_c x_s)j$ [11]. In the fixed-axis gear section, the translational vibration acceleration of the fixed-axis gears contains only the translational acceleration, e.g., the position of gear 1 is $r_1 = x_1 i + y_1 j$, and the translational acceleration of gear 1 is $\ddot{r}_1 = \ddot{x}_1 i + \ddot{y}_1 j$. The equations of motion of the components of the planetary gear are shown below.

The equation of motion of the sun gear is as follows:

$$\begin{cases} m_s(\ddot{x}_s - y_s\ddot{\theta}_c) = \sum_{n=1}^{3} F_{spn}\sin\psi_{spn} - k_{bs}x_s - c_{bs}\dot{x}_s \\ m_s(\ddot{y}_s + x_s\ddot{\theta}_c) = -\sum_{n=1}^{3} F_{spn}\cos\psi_{spn} - k_{bs}y_s - c_{bs}\dot{y}_s \\ J_s(\ddot{\theta}_s + \ddot{\theta}_c) = -\sum_{n=1}^{3} F_{spn}r_s + T_L \end{cases} \quad (1)$$

The equations of motion of planetary gears are as follows:

$$\begin{cases} m_p(\ddot{x}_{pn} - y_{pn}\ddot{\theta}_c) = F_{spn}\sin\alpha_{spn} - F_{rpn}\sin\alpha_{rpn} \\ \qquad + k_{bpn}\delta_{cpnx} + c_{bpn}\dot{\delta}_{cpnx} \\ m_p(\ddot{y}_{pn} + x_{pn}\ddot{\theta}_c) = F_{spn}\cos\alpha_{spn} + F_{rpn}\cos\alpha_{rpn} \\ \qquad + k_{bpn}\delta_{cpny} + c_{bpn}\dot{\delta}_{cpny} \\ J_p\ddot{\theta}_{pn} = (F_{rpn} - F_{spn})r_p \end{cases} \quad (2)$$

The equation of motion of the ring is as follows:

$$\begin{cases} m_r(\ddot{x}_r - y_r\ddot{\theta}_c) = \sum_{n=1}^{3} F_{rpn}\sin\psi_{rpn} - k_{br}x_r - c_{br}\dot{x}_r \\ m_r(\ddot{y}_r + x_r\ddot{\theta}_c) = -\sum_{n=1}^{3} F_{rpn}\cos\psi_{rpn} - k_{br}y_r - c_{br}\dot{y}_r \\ J_r(\ddot{\theta}_r + \ddot{\theta}_c) = T_1 - \sum_{n=1}^{3} F_{rpn}r_r \end{cases} \quad (3)$$

where, $\delta_{spn}, \delta_{rpn}$ represents the compression deformation between the nth planetary gear and the sun gear or ring respectively, and $\delta_{cpnx}, \delta_{cpny}$ represents the radial and tangential compression deformation between the planetary gear bearing and the carrier, expressed as follows:

$$\begin{aligned} \delta_{spn} &= r_s\theta_s - x_s\sin\psi_{spn} + y_s\cos\psi_{spn} + r_{pn}\theta_{pn} \\ &\quad -x_{pn}\sin\alpha_{spn} - y_{pn}\cos\alpha_{spn} \\ \delta_{rpn} &= r_r\theta_r - x_r\sin\psi_{rpn} + y_r\cos\psi_{rpn} - r_{pn}\theta_{pn} \\ &\quad +x_{pn}\sin\alpha_{rpn} - y_{pn}\cos\alpha_{rpn} \\ \delta_{cpnx} &= x_c\cos\psi_n + y_c\sin\psi_n - x_{pn} \\ \delta_{cpny} &= y_c\cos\psi_n - x_c\sin\psi_n - y_{pn} \end{aligned} \quad (4)$$

where ψ_n represents the position angle of the nth planetary gear distributed along the circumference of the carrier, represent the meshing angle of the sun gear or ring with the nth planetary gear, and ψ_{spn}, ψ_{rpn} represent the angle between the direction of the line of the mesh of the sun gear or ring with the nth planetary gear and the axis, respectively.

$$\begin{cases} \psi_n = 2\pi(n-1)/N \\ \psi_{spn} = \psi_n - \alpha_{spn} \\ \psi_{rpn} = \psi_n + \alpha_{rpn} \end{cases} \quad (5)$$

The equations of motion of the components of the fixed shaft gears are as follows:

$$\begin{cases} m_1\ddot{x}_1 = (k_{12}\delta_{12} + c_{12}\dot{\delta}_{12})\sin\alpha_{12} - k_{b1}x_1 - c_{b1}\dot{x}_1 \\ m_1\ddot{y}_1 = -(k_{12}\delta_{12} + c_{12}\dot{\delta}_{12})\cos\alpha_{12} - k_{b1}y_1 - c_{b1}\dot{y}_1 \\ J_1\ddot{\theta}_1 = T_2 + (k_{12}\delta_{12} + c_{12}\dot{\delta}_{12})r_1 \end{cases} \tag{6}$$

The remaining equations for fixed shaft gear dynamics can be found in Ref. 13 which is not described here [13].

The member c is a composite member of the carrier and gear 4 and is subject to both the forces of the planetary gears on the carrier and the meshing forces of gear 7 and gear 3, with the following equations of motion:

$$\begin{cases} m_c(\ddot{x}_c - y_c\ddot{\theta}_c) = \sum_{n=1}^{N} k_{bpn}\delta_{cpny}\sin\psi_n \\ \qquad\qquad - \sum_{n=1}^{N} k_{bpn}\delta_{cpnx}\cos\psi_n \\ \qquad\qquad -F_{34}\sin\alpha_{34} + F_{74}\sin\alpha_{74} - k_{bc}x_c \\ m_c(\ddot{y}_c + x_c\ddot{\theta}_c) = -\sum_{n=1}^{N} k_{bpn}\delta_{cpnx}\sin\psi_n \\ \qquad\qquad - \sum_{n=1}^{N} k_{bpn}\delta_{cpny}\cos\psi_n \\ \qquad\qquad F_{74}\cos\alpha_{74} - F_{34}\cos\alpha_{34} - k_{bc}y_c \\ (J_c + 3J_{pc})\ddot{\theta}_c = -F_{34}r_4 - F_{74}r_4 - r_c\sum_{n=1}^{N} k_{bpn}\delta_{cpny} \end{cases} \tag{7}$$

$k_{bj}(j = s, r, c, 1, 2, 3, 5, 6, 7, p1, \ldots pN)$ is the support stiffness of the bearing to each member, $c_{bj}(j = s, r, c, 1, 2, 3, 5, 6, 7, p1, \ldots pN)$ is the support damping of the bearing to each member, T_1, T_2, T_3 is the input torque of the ring, gear 1 and gear 5 respectively, and also the load torque of the three motors, expressed as $T_1 = k_1(\theta_{M1} - (\theta_r + \theta_c))T_2 = k_2(\theta_{M2} - \theta_1)T_3 = k_3(\theta_{M3} - \theta_5)$.

The time-varying meshing stiffness of the fixed shaft gear and planetary gear system is more conveniently expressed by the following equation [13]:

$$\begin{aligned} k_{spn}(\theta_{pn}) &= \bar{k}_{spn} + \sum_{i=1}^{\infty} a_l\cos[l(Z_p\theta_{pn} + Z_s\psi_n + \gamma_{spn} + \gamma_{sr})] \\ k_{12}(\theta_1) &= \bar{k}_{12} + \sum_{i=1}^{\infty} a_l\cos[l(Z_1\theta_1 + \gamma_{12})] \end{aligned} \tag{8}$$

where $\bar{k}_j(j = spn, rpn, 12, 34, 56, 74)$ is the average meshing stiffness for one meshing cycle, calculated via ISO 6336-1-2006, a_l is the Fourier expansion factor, l is the number of harmonics, γ_j is the phase angle of the meshing stiffness, γ_{sr} is the phase angle difference between the inner and outer meshes of the same planetary gear, $\gamma_{sr} = 0$ when the number of planetary wheel teeth is odd and $\gamma_{sr} = \pi$ when the number of planetary wheel teeth is even.

The expression for the mesh damping is as follows [14]:

$$c_{pq} = 2\zeta_{pq}\sqrt{\bar{k}_{pq}m_pm_q/(m_p + m_q)} \tag{9}$$

where ζ_{pq} is the mesh damping ratio and m_p, m_q is the mass of gear p, gear q respectively.

The mechanical characteristics of the fan and pump loads are [24]:

$$T_L = k\omega^2 + ad\omega/dt + b\omega + c \tag{10}$$

where ω is the fan or pump speed, k is the fluid resistance torque coefficient, b is the viscous manufacturing resistance torque coefficient, c is the potential torque coefficient, a is the inertia torque coefficient, the steady state load torque is mainly determined by the fluid resistance torque of the fan/pump load, the expression is as follows:

$$T_L = k\omega^2 \tag{11}$$

III. MODEL OF THE MOTOR BY THE EQUIVALENT CIRCUIT METHOD

The motor acts as a hub connecting the power supply and mechanical part and in order to study the complete electromechanical coupling dynamic characteristics, it is necessary to model the electromagnetic dynamics of the motor. Currently, the most straightforward way to accurately model the motor is to use the finite element method for analysis, but when it comes to co-simulation with other systems, the finite element method becomes less practical. It is possible to decouple this by making reasonable assumptions and using a set of linear differential equations of the same order containing the voltage equation, the magnetic chain equation, and the electromagnetic torque equation to describe the electromagnetic dynamics of the motor [25] In this section, the Park transform is used to describe the motor by modeling the equivalent circuit in the motor rotating d-q coordinate system, the equivalent circuit is shown in Fig. 3 [26].

The corresponding voltage equations for the stator and rotor of the motor are:

$$\begin{cases} u_{ds} = R_si_{ds} + \dfrac{\mathrm{d}}{\mathrm{d}t}\psi_{ds} - \omega\psi_{qs} \\ u_{qs} = R_si_{qs} + \dfrac{\mathrm{d}}{\mathrm{d}t}\psi_{qs} + \omega\psi_{ds} \\ u_{dr} = R_ri_{dr} + \dfrac{\mathrm{d}}{\mathrm{d}t}\psi_{dr} - (\omega - \omega_r)\,\psi_{qr} \\ u_{qr} = R_ri_{qr} + \dfrac{\mathrm{d}}{\mathrm{d}t}\psi_{qr} + (\omega - \omega_r)\,\psi_{dr} \end{cases} \tag{12}$$

where the subscripts d and q denote the d-axis quantities and q-axis quantities respectively, the subscripts s and r denote the stator and rotor quantities respectively, u, i, R is the voltage, current and resistance respectively, ω, ω_r are the rotor mechanical angular velocity and rotor electromagnetic angular velocity respectively, ψ is the flux, and the equation

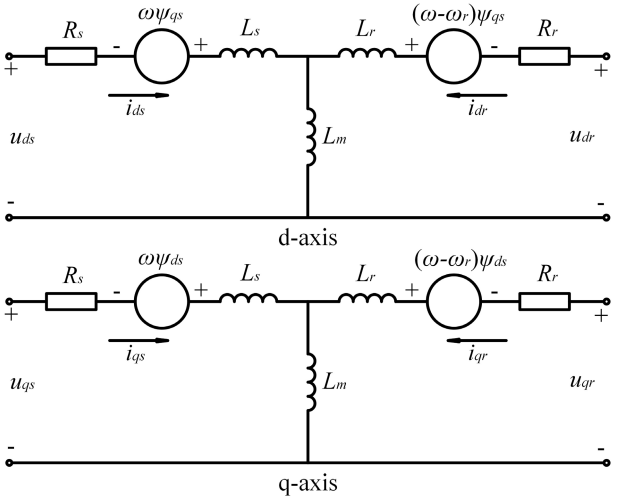

FIGURE 3. Equivalent circuit in the d-q coordinate system of the motor.

for the flux of the stator and rotor is:

$$\begin{cases} \psi_{ds} = L_s i_{ds} + L_m i_{dr} \\ \psi_{qs} = L_s i_{qs} + L_m i_{qr} \\ \psi_{dr} = L_m i_{ds} + L_r i_{dr} \\ \psi_{qr} = L_m i_{qs} + L_r i_{qr} \end{cases} \tag{13}$$

where L_s, L_r are the stator and rotor winding leakage inductance respectively and L_m is the magnetizing inductance.

The generation of electromagnetic torque in a motor is essentially based on the interaction of magnetic flux and current and is given by the following equation:

$$T_e = 1.5p(\psi_{ds} i_{qs} - \psi_{qs} i_{ds}) \tag{14}$$

where T_e is the electromagnetic torque and p is the number of poles in the motor.

IV. UNITS

As the auxiliary motor requires speed regulation, the auxiliary motor power supply needs to be regulated by an inverter. The principle is shown in Fig. 4, where the reference voltage and reference frequency required for system speed regulation is calculated through constant voltage to frequency (V/f) control, and the signal generated by sine pulse width modulation (SPWM) drives the inverter to generate the required inverter power to drive the motor and achieve speed regulation.

V/f control is an open-loop control method for keeping the ratio of the amplitude of the induced electric potential on the stator side to the frequency constant in order to maintain a constant magnetic flux and is the best choice for simple variable-speed applications such as fans and pumps [19]. The voltage versus frequency of the auxiliary motor after considering the compensation voltage is as follows:

$$u(f) = \frac{u_N - u_0}{f_N} f + u_0 \tag{15}$$

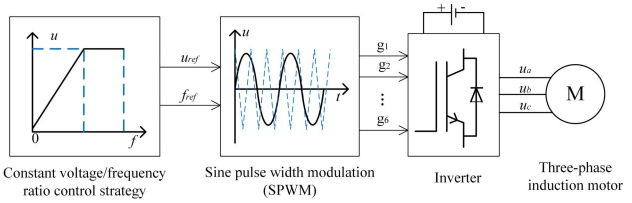

FIGURE 4. Inverter power supply drive principle.

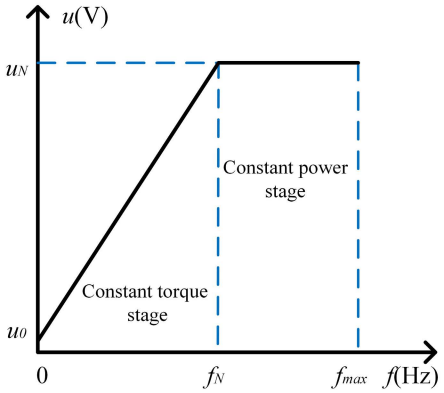

FIGURE 5. Stator voltage versus supply frequency under V/f control.

where u_N is the rated voltage of the motor, f_N is the rated frequency of the motor, u_0 is the voltage to compensate for the voltage drop of the stator resistance during starting. The operating curve of voltage and frequency is shown in Fig. 5. As can be seen from Fig. 5, below the rated frequency f_N is V/f control, the flux basically remains the constant, above the rated frequency f_N, the voltage does not increase with the frequency, for the constant power stage.

The input to the SPWM is three sinusoidal reference voltages with a phase interval of 120 degrees. The triangular carrier signals u_Δ are compared with the corresponding reference signals u_{ref} to produce the gating signal for that phase, and the generation mechanism is shown in Fig. 6. The carrier signal is compared with the reference voltage u_a, u_b, u_c to obtain g_1, g_3, g_5,respectively, and the non-getting g_2, g_4, g_6 of g_1, g_3, g_5 is taken, which together form the PWM waveform.

The inverter consists of six power switching devices IGBTs [28], as shown in Fig. 7. The V/f control and SPWM output pulses are used to control the power switching devices IGBTs to turn on or off to adjust the output three-phase AC voltage and current magnitude, thus realizing the drive control of the load.

The inverted three-phase voltage after SPWM and inverter with the reference three-phase voltage is shown in Fig. 8.

V. STUDY OF DYNAMIC CHARACTERISTICS UNDER VARIABLE WORKING CONDITIONS

In this study, the dynamic model for the electromechanical coupled system consisting of inverter power supply,

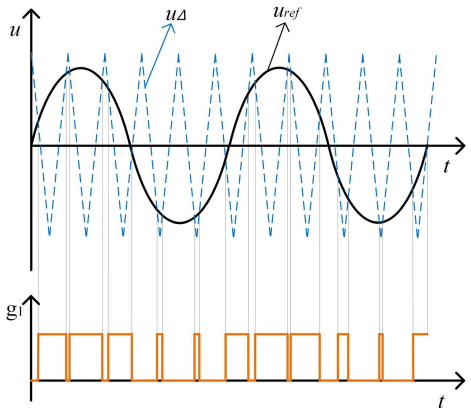

FIGURE 6. SPWM generation principle.

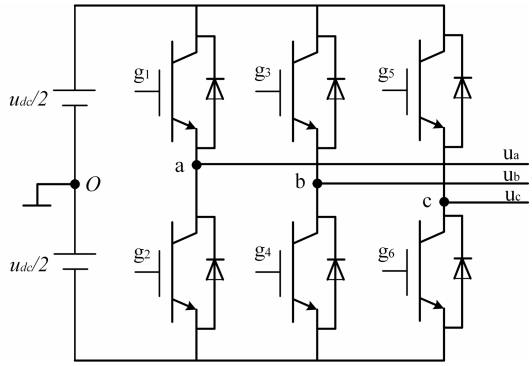

FIGURE 7. Inverter model.

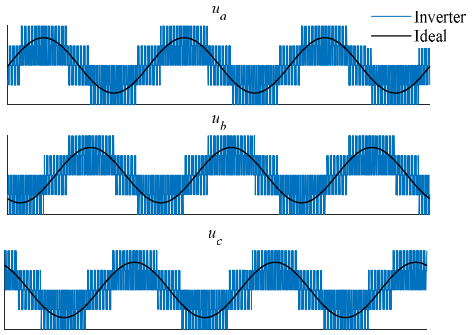

FIGURE 8. Inverter and ideal power supplies.

three-phase asynchronous motors, differential planetary gear system and pump load is established. The dynamic characteristics of the coupled electromechanical system are analyzed under the conditions of start-up, steady-state, and speed regulation.

The planetary differential gear system model considering time-varying meshing stiffness and damping was built in Matlab/Simulink by S-function. The gear model is connected with V/f control, SPWM generator, inverter and Asynchronous Machine in Matlab/Simulink, where the inverter generates the inverted voltage directly as an input to the

TABLE 1. Parameters of the gear train.

Gear symbol	Sun gear	Planet gear	Ring gear	Gear 1(5)	Gear 2(6)	Gear 3(7)	Gear4 (carrier)
Teeth number	43	74	191	21	57	58	131
Module (mm)	8						
Mass(kg)	3.55	4.50	6.92	1.60	4.14	4.17	8.35
J(kg·m^2)	0.046	0.174	1.78	0.005	0.095	0.099	1.01
Bearing stiffness(N/m)			10^9				
Bearing damping(N·s/m)			10^4				
Average mesh stiffness (N/m)			7×10^8				
Mesh damping(N·s/rad)			10^4				
Shaft stiffness(N/rad)			$k_1=k_2=k_3=10^8$ $k_4=k_5=10^9$				

TABLE 2. Parameters of the motors.

	Main motor	Auxiliary motor 1 (2)
Stator resistance R_s (Ω)	0.02475	0.2761
Stator inductance L_s (H)	0.000284	0.002191
Rotor resistance R_r (Ω)	0.01329	0.1645
Rotor inductance L_r (H)	0.000284	0.002191
Mutual inductance L_m (H)	0.01425	0.07641
Friction factor F (N·m·s)	0.06346	0.01771

TABLE 3. Parameters of the power supply.

Parameter	Main motor	Auxiliary motor
Rated voltage U_N (V)	575	460
Rated frequency f_N (Hz)	60	60
Rated power P (Kw)	149	14.9
Compensation voltage U_0 (V)	/	20
Triangular carrier amplitude U (V)	/	500
Triangular carrier frequency f_c (Hz)	/	2500

motor, and the motor is connected to the gear system by electromagnetic torque and torque on the motor shaft with the following differential equations:

$$J_{Mn}\ddot{\theta}_{Mn} = T_{en} - T_n - F_n\theta_{Mn} \tag{16}$$

where the subscript n = 1,2,3 represents the main motor and the two auxiliary motors respectively, T_{en} is the electromagnetic torque of the nth motor and T_n is the load torque of the nth motor, for which the formula F is the coefficient of viscous friction and θ_{Mn} is the angle of rotation of the nth motor, as already given in Section 2.

The main parameters of the electromechanically coupled differential speed regulation system are as follows.

A. START-UP STAGE

In previous studies of electromechanical coupling, the influence of the inverter part was not considered and the power supply to the motor was simplified to an ideal three-phase supply direct drive (DD). In the variable frequency drive (VFD), the voltage frequency of the starting process is

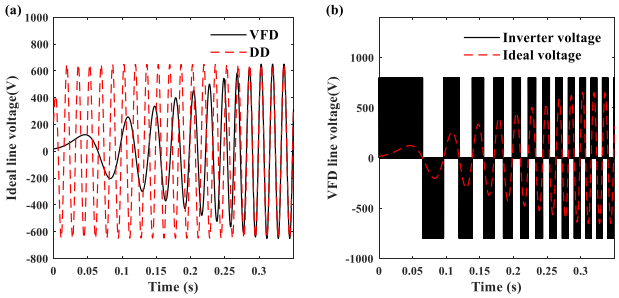

FIGURE 9. Auxiliary motor line voltage: (a) comparison of ideal voltage under VFD and DD, (b)comparison of inverted voltage and ideal voltage under VFD.

gradually increased from 0 to the rated frequency. The ideal line voltage of the auxiliary motor is shown in Fig. 9(a) for both models of the variable frequency drive and the direct drive, where the amplitude and frequency of the voltage in the variable frequency drive are continuously increased under constant voltage to frequency ratio control (V/f), while the amplitude and frequency of the supply voltage in the direct drive are constant. Due to the inverter, the inverted line voltage is plotted against the ideal line voltage as shown in Fig. 9(b).

The main motor starts under DD, the main motor starts under DD and the auxiliary motors are driven with VFD and DD. Driven by the drive voltage, the motor startup characteristics are shown in Fig. 10. As can be seen in Fig. 10(a), the electromagnetic torque of the auxiliary motor under VFD fluctuates more smoothly than DD until 0.2s, the time to reach the peak torque is shorter and the peak is lower than DD, as a result of the uniform rise in voltage and frequency of the supply using the VFD, but the presence of the inverter increases the harmonic content of the electromagnetic torque and makes it more volatile. The load torque of the motor is shown in Fig. 10(b). The load torque is the link between the gear system and the motor system, during the start-up process, the load torque on the motor shaft will produce shocks, and the shocks are produced earlier under VFD than DD, and the load torque vibration trend during the start-up process basically matches the electromagnetic torque. Fig. 10(c) shows the auxiliary motor speed. It can be seen that the motor speed takes less time to reach steady state with VFD than DD, and that there is a reduction and then increase in motor speed at 3.1s, which is related to the increase and then decrease in torque amplitude at 3.1s in Fig. 10(a) and Fig. 10(b). As can be seen in Fig. 10(d), the motor stator current is significantly lower than that of the DD during start-up, resulting in a smaller impact on the electrical network. From Fig. 10(a), (b) and (d) it can be seen that the amplitude of the electromagnetic torque, load torque and stator current keep growing steadily after violent fluctuations and reaches a steady state after 3s. This is caused by the fact that the main motor speed under DD is increasing as in Fig. 10(e) and the speed of the sun gear is increasing, resulting in the increasing system load torque as in Fig. 10(f) due to

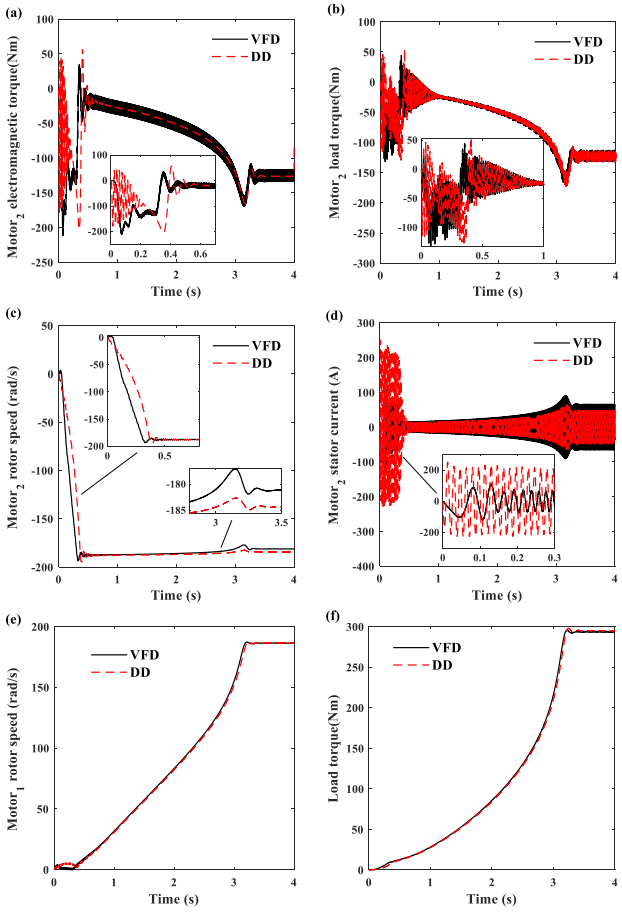

FIGURE 10. Auxiliary motor: (a) electromagnetic torque, (b) load torque, (c) rotor speed, (d) stator current; (e) rotor speed of the main motor, (f) total system load.

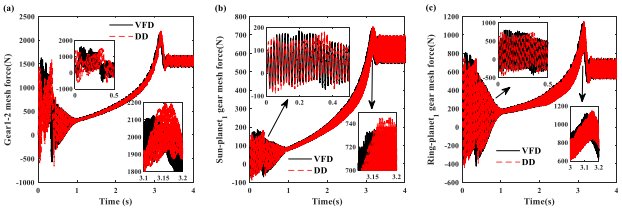

FIGURE 11. (a) Fixed shaft gear meshing force, (b) sun gear-planetary gear meshing force, (c) ring-planetary gear meshing force.

the load torque of the fan and pump being proportional to the square of the speed.

During the start-up of the differential speed regulation system, the meshing forces between the fixed shaft gears and the planetary gears are shown in Fig. 11. Fig. 11(a) shows the meshing forces between gear 1 and gear 2 directly connected to the auxiliary motor, Fig. 11(b) shows the meshing forces between the sun gear and planetary gear 1, and Fig. 11(c) shows the meshing forces between the ring and planetary gear 1. These three meshing forces basically coincide with the overall trend in the start-up transient values, and the start-up process before 1s shows that the system is preceded at peak and valley start-up values by VFD. During the period

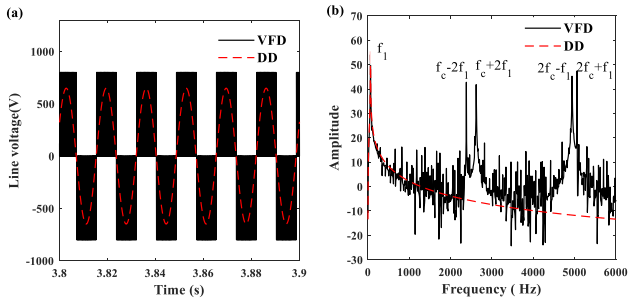

FIGURE 12. Comparison of auxiliary motor supply voltages at steady state: (a) time domain; (b) frequency domain.

1s-3s the meshing forces increase, this is due to the fact that the system speed is increasing and the load torque is rising, after 3s the VFD has a smaller peak compared to DD before reaching a steady state.

B. STEADY-STATE STAGE

After reaching a steady state, the time domain diagrams of the auxiliary motor supply line voltage for the two drive models are shown in Fig. 12(a), where the supply voltage in the VFD is the inverter voltage generated through the inverter and the supply voltage in the DD is the ideal sinusoidal voltage. The spectrum of the voltage is shown in Fig. 12(b), the power supply fundamental frequency f_1 is the dominant frequency, near f_1 the spectral characteristics of the two are basically the same, but at high frequencies, the ideal voltage approximates a smooth curve, the inverter voltage spectrum contains more harmonic components, which peaks at the modulation frequency $f_c \pm 2f_1, 2f_c \pm f_1$ resulting from the coupling of the delta carrier frequency with the power supply fundamental frequency.

The spectrum of electromagnetic torque, load torque, rotor speed and stator current of the auxiliary motor when the system reaches a steady state is shown in Fig. 13. The frequency diagram of the electromagnetic torque of the motor is shown in Fig. 13(a). Due to the presence of the inverter, the electromagnetic torque under VFD contains a richer harmonic component, including the frequency component $f_c \pm 3f_1, 2f_c \pm f_1, 2f_c$ generated by the inverter, in addition to the fixed shaft gear meshing frequency f_m1, which coincides with the DD. Fig. 13(b) shows the load torque spectrum with the direct drive spectrum containing the fixed shaft gear meshing frequency f_m1 and its multiples, and the inverter drive spectrum containing the $f_c \pm 3f_1, 2f_c$ harmonic component generated by the inverter in addition to the frequency components contained in the direct drive. The rotor speed spectrum in Fig. 13(c) shows that the frequency components are essentially similar to those in Fig. 13(b). The rotor speed spectrum under VFD contains both the gear meshing frequency harmonics and the inverter harmonic components. The motor stator current spectrum is shown in Fig. 13(d). The spectral characteristics are similar to those of the voltage spectrum in Fig. 12(b) but are smoother at higher frequencies than in Fig. 12(b), due to the electromagnetic

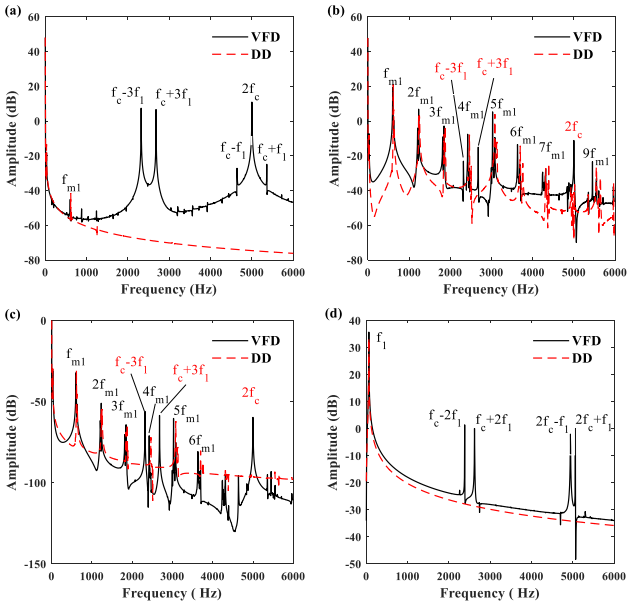

FIGURE 13. Auxiliary motor spectrum: (a) electromagnetic torque, (b) load torque, (c) rotational speed, (d) stator current.

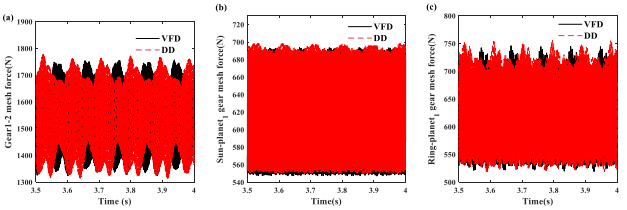

FIGURE 14. (a) Fixed shaft gear meshing force, (b) sun gear - planetary gear meshing force, (c) ring - planetary gear meshing force.

effect of the motor, which attenuates the harmonic effects of the inverter. The above spectrum shows that the motor system is affected by the coupling of the gear mesh harmonics and the inverter harmonics, indicating that the relationship between the two should be fully considered when designing the system to avoid resonance between the two harmonics in close proximity.

The gear meshing force at a steady state is shown in Fig.14. The peak meshing force at steady-state with variable frequency drive is slightly smaller than with direct drive, and no further difference can be seen in the meshing force time-domain diagram, which is analyzed in the meshing force spectrum below.

Fig. 15(a) shows the frequency spectrum of the meshing force of the fixed shaft gear. The spectrum shows that under DD without an inverter, the frequency component of the fixed shaft gear meshing force is mainly the fixed shaft gear mesh fundamental frequency and its multiplier $nf_{m1}(n = 1, 2, 3 \ldots)$. Under VFD, the frequency of the fixed shaft gear mesh force component includes not only the mesh fundamental frequency and its multiplier but also the $f_c \pm 3f_1, 2f_c$ frequency component generated by the inverter. Fig. 15(b) shows the spectrum of the meshing force

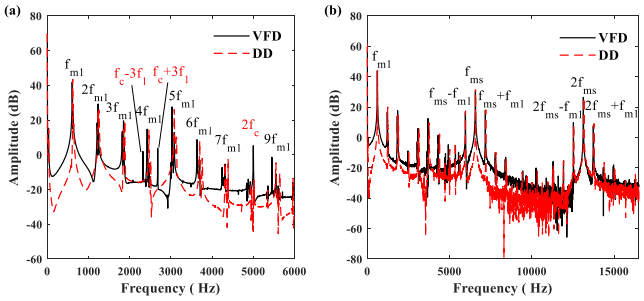

FIGURE 15. (a) Fixed shaft gear meshing force spectrum, (b) sun gear - planetary gear 1 meshing force spectrum.

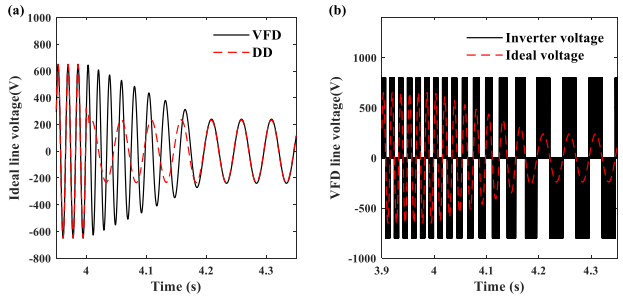

FIGURE 16. Auxiliary motor line voltage: (a) comparison of ideal voltage under VFD and DD, (b) comparison of inverted voltage and ideal voltage under VFD.

of the sun gear and the planetary gear. From the figure, it can be seen that the components of the meshing force spectrum match under VFD and DD, mainly containing the meshing frequency of the fixed shaft gear and its multiplier $nf_{m1}(n = 1, 2, 3\ldots)$, the meshing frequency of the planetary gear and its multiplier $nf_{ms}(n = 1, 2\ldots)$ as well as the modulation frequency $f_{ms} \pm f_{m1}, 2f_{ms} \pm f_{m1}$ of both. The inverter effect on the frequency of the planetary gear meshing force is barely visible because the harmonics generated by the inverter are transmitted to the carrier via the fixed shaft gear, attenuating the effect of the inverter harmonics in the transmission process. For the gear meshing forces directly connected to the auxiliary motor, the inverter harmonics have a greater influence.

C. SPEED-DOWN STAGE

When the system meets the process requirements, the speed needs to be reduced, keep the main motor speed constant, through the constant voltage to frequency ratio control of the auxiliary motor voltage and frequency smoothly reduced, VFD and DD ideal line voltage as shown in Fig. 16 (a), the voltage amplitude and frequency change abruptly with DD and transition smoothly with VFD. The inverter voltage and the ideal voltage in the VFD are shown in Fig. 16(b).

The dynamic characteristics of the motor during speed regulation are shown in Fig.17. As can be seen in Fig. 17(a), under direct drive, the voltage amplitude and frequency change abruptly, resulting in a large shock to the auxiliary motor electromagnetic torque, and there are also large fluctuations in amplitude after the shock, while under variable

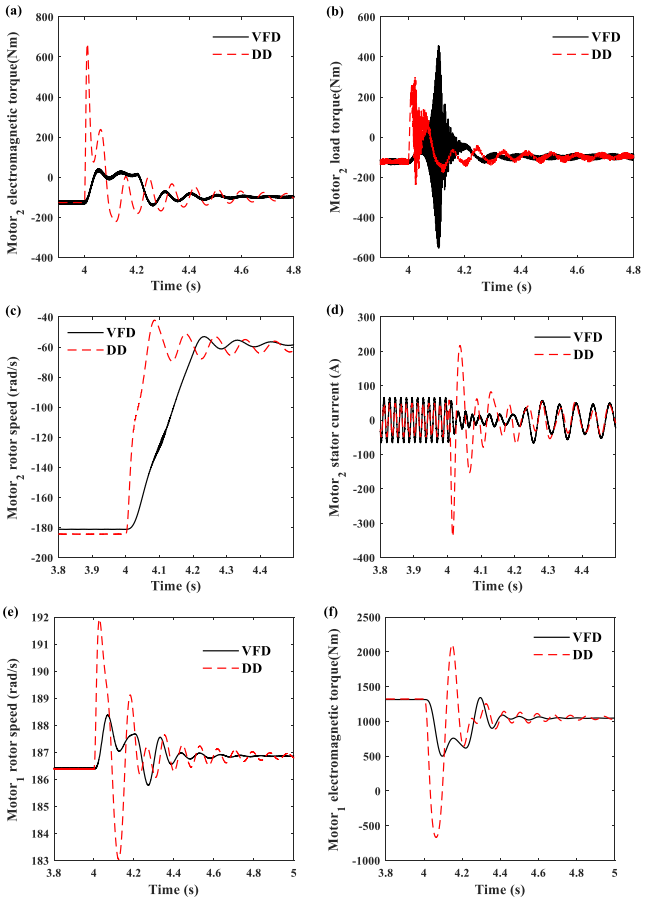

FIGURE 17. Auxiliary motor: (a) electromagnetic torque, (b) load torque, (c) rotor speed, (d) stator current; main motor: (e) rotor speed, (f) electromagnetic torque.

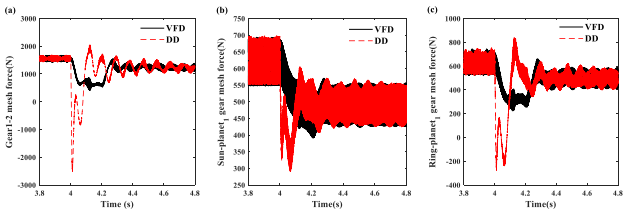

FIGURE 18. (a) Fixed shaft gear meshing force, (b) sun gear - planetary gear meshing force, (c) ring - planetary gear meshing force.

frequency drive the motor electromagnetic torque changes more smoothly, and the time required to reach steady state is short, and the fluctuations under steady state are small. As the electromagnetic torque decreases, the rotor speed of the auxiliary motor Fig. 17(c) also decreases. The speed changes more evenly and the time required to reach the new steady state is longer and less volatile under VFD, the time required to reach the steady state is shorter but more volatile under DD. The trends in motor load torque Fig.17(b) and electromagnetic torque Fig.17(a) largely coincide, with the load torque containing more vibrations and harmonics due to the electromagnetic effect of the motor attenuating the harmonics and vibrations of the electromagnetic torque.

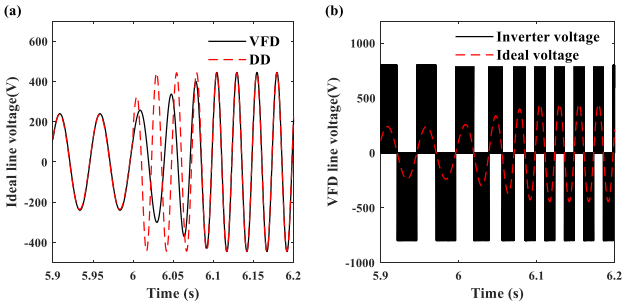

FIGURE 19. Auxiliary motor line voltage: (a) comparison of ideal voltage under VFD and DD, (b) comparison of inverted voltage and ideal voltage under VFD.

As can be seen in Fig. 17(d) for the auxiliary motor stator current, direct changes in voltage amplitude and frequency under DD cause the stator current to surge, while slow changes in voltage amplitude and frequency under VFD cause the current to vary more gently. During the auxiliary motor for speed regulation, the main motor rotor speed is shown in Fig.17(e), due to the auxiliary motor speed regulation process caused a load shock change, resulting in the main motor rotor speed also a shock, after the shock the main motor speed is slightly higher, caused by the main motor load torque reduction after speed regulation, the electromagnetic torque of the main motor is shown in fig. 17(f), after speed regulation the electromagnetic torque is reduced, the power is reduced, to achieve the purpose of energy-saving.

During speed regulation, the gear meshing force changes as shown in Fig. 18. As the speed decreases, corresponding to lower system load torque, the meshing force between the gears also decreases. Fig. 18(a) shows the meshing force between the fixed shaft gear 1 and gear 2. The gear meshing force varies relatively smoothly under VFD, with no obvious shocks, which is a similar trend to the electromagnetic torque Fig. 17(a) and the load torque Fig. 17(b) of the auxiliary e motor. Fig. 18(b) shows the meshing force between the sun gear and planetary gear 1. The meshing force decreases smoothly under VFD, while a sudden change in meshing force resulting in shock can occur under DD.

D. SPEED-UP STAGE

When the system speed needs to be increased, similar to the speed-down stage, the main motor is kept constant and the variable frequency drive smoothly increases the voltage and frequency of the auxiliary motor through constant voltage to frequency ratio control, and the direct drive changes abruptly to the target frequency. The ideal line voltage under both drives is shown in Fig. 19(a), the inverter voltage and the ideal voltage under VFD is shown in Fig. 19(b).

The dynamic characteristics of the motor during the speed-up process are shown in Fig. 20. As can be seen in Fig. 20(a), the electromagnetic torque of the auxiliary motor changes smoothly under VFD, while a temporary shock is generated under DD due to sudden changes in frequency. Fig. 20(b) shows the load torque of the auxiliary motor,

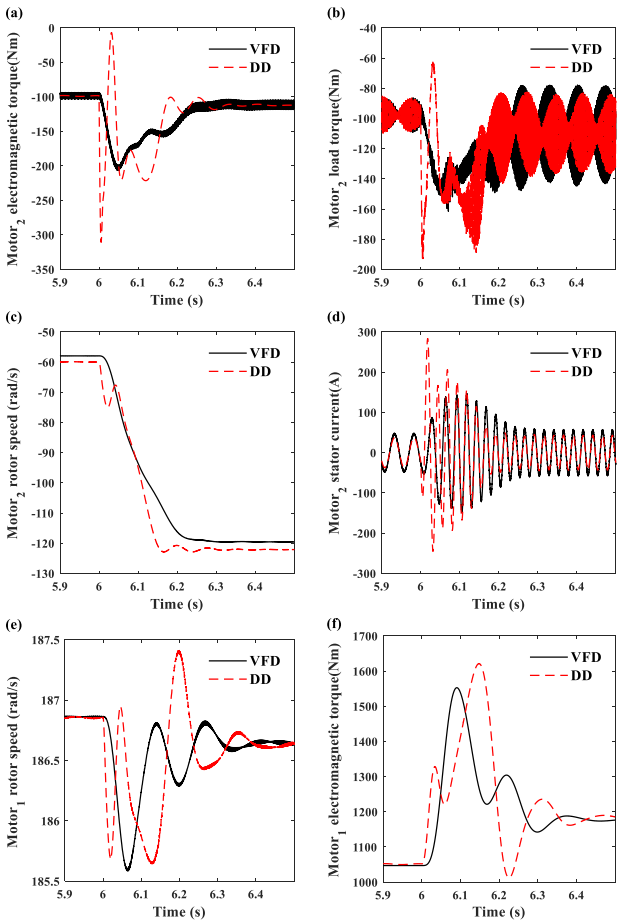

FIGURE 20. Auxiliary motor: (a) electromagnetic torque, (b) load torque, (c) rotor speed, (d) stator current; main motor: (e) rotor speed, (f) electromagnetic torque.

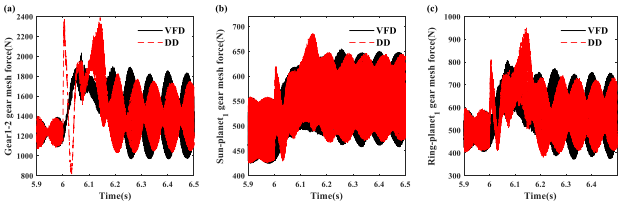

FIGURE 21. (a) Fixed shaft gear meshing force, (b) sun gear - planetary gear meshing force, (c) ring - planetary gear meshing force.

with a similar trend to the electromagnetic torque, but with greater amplitude of vibration than in Fig. 20(a), due to the electromagnetic effect of the motor as mentioned in several processes above. Fig. 20 (c) shows the rotor speed of the auxiliary motor. Under DD, the rotor speed of the auxiliary motor appears to decrease and then increase at around 6.05s, which is related to the sudden change in torque in Fig. 20(a)(b), compared to the smooth change in speed under VFD. Fig. 20(d) shows the stator current of the auxiliary motor. As can be seen in fig. 19, the voltage and frequency increase from low to high to the rated value under both drives, but the amplitude of the motor's stator current increases to a peak value larger than the rated value and then decreases to the rated value, which is the similar

trend as the load torque of the auxiliary motor in Fig. 20(b). It shows that the stator current is not only influenced by the amplitude and frequency of the power supply, but also by the mechanical load. During the speed-up of the auxiliary motor, the main motor rotor speed, as shown in Fig. 20 (e), fluctuates temporarily and then drops slightly, as a result of the fluctuation and then rise of the main motor load torque during speed regulation as shown in Fig. 20 (f).

The meshing forces during the speed-up process are shown in Fig. (21). During the speed regulation process, the direct drive will have a large shock at around 6.05s and 6.15s for all three meshing forces, and then tends to stable, which coincides with the impact of the auxiliary motor electromagnetic torque, load torque, main motor rotor speed and electromagnetic torque, and it is the impact of the motor electromagnetic torque that causes the impact of the gear meshing forces. After the speed increase, the vibration amplitude of the three meshing forces is more intense than before the speed regulation, indicating that the choice of system speed is very important for the vibration characteristics of the electromechanically coupled system.

VI. CONCLUSION

In the dynamic analysis of electromechanical systems, it is important to accurately model the whole system and to analyze the dynamic characteristics of the steady state and transients for design improvement and health monitoring. In this paper, the electromechanical coupled system model with inverter power supply, three-phase induction motor, differential planetary gears and load is established. The differences of the dynamic characteristics of the electromechanical system under the variable frequency drive (VFD) model and the direct drive (DD) model are investigated, where the VFD model includes constant voltage to frequency ratio control, sinusoidal pulse width modulation (SPWM) and inverter, and the DD model is a simplified model considering an ideal power supply. The dynamic characteristics of the electromechanical coupling of the system during the start-up, steady-state, speed-down and speed-up stages are analyzed.

With the VFD model, the drive voltage of the three-phase asynchronous motor is more complex and contains more harmonics due to the presence of the SPWM and inverter. In the start-up stage, the induction motor of the VFD model reaches steady state faster and fluctuates more smoothly than the DD model, but the electromagnetic torque under VFD model contains more harmonic components, and the time domain meshing forces of the gear system do not differ much, both vibrating first and then steadily increasing to steady state values. During the speed regulation stage, the frequency and voltage of the supply are uniformly changed under VFD model, making the process smooth and with relatively low shock vibration. Compared to DD model, the VFD model reflects the transient dynamic characteristics of the system in a more realistic and rational form.

In the steady state stage, we can see from the auxiliary motor electromagnetic torque spectrum diagram that the motor is affected by the coupling of the inverter harmonics in the power supply section and the gear meshing harmonics in the mechanical section. The VFD model has a richer harmonic component than the DD model, which is reflected in the electromagnetic torque, motor rotor speed, stator current, and the gear meshing forces directly connected to the auxiliary motor. This indicates that the interaction between the carrier frequency and the fundamental frequency of the power supply section and the gear meshing frequency of the mechanical section should be fully considered when designing the planetary gear or selecting the inverter. A suitable speed should also be selected to avoid resonance due to the similarity of the harmonic frequencies of the two.

Inverter harmonics can have a coupling effect on the electromechanical system. In addition, gear faults can also affect the dynamic characteristics of the mechatronic system, and the effects of gear faults on the mechatronic system will be further investigated in the next step.

REFERENCES

[1] R. Saidur, N. A. Rahim, and M. Hasanuzzaman, "A review on compressed-air energy use and energy savings," *Renew. Sustain. Energy Rev.*, vol. 14, no. 4, pp. 1135–1153, May 2010.

[2] R. Saidur, S. Mekhilef, M. B. Ali, A. Safari, and H. A. Mohammed, "Applications of variable speed drive (VSD) in electrical motors energy savings," *Renew. Sustain. Energy Rev.*, vol. 16, no. 1, pp. 543–550, Jan. 2012.

[3] C. Tan, Z.-M. Feng, X. Liu, J. Fan, W. Cui, R. Sun, and Q. Ma, "Review of variable speed drive technology in beam pumping units for energy-saving," *Energy Rep.*, vol. 6, pp. 2676–2688, Nov. 2020.

[4] R. Saulescu, C. Jaliu, and D. Ciobanu, "Differential planetary gear transmissions usable in renewable energy systems," *Mech., Transmiss. Appl.*, vol. 2012, pp. 273–280, Feb. 2012.

[5] M. Teitel, A. Levi, Y. Zhao, M. Barak, E. Bar-Lev, and D. Shmuel, "Energy saving in agricultural buildings through fan motor control by variable frequency drives," *Energy Buildings*, vol. 40, no. 6, pp. 953–960, Jan. 2008.

[6] S. Wang, M. Sheng, and D. Hu, "Energy-saving analysis and calculation of HV frequency conversion retrofitting for fan and pump," *Electr. Power Autom. Equip.*, vol. 3, pp. 1–15, Mar. 2011.

[7] W. Shuping, "Energy efficiency evaluation investigation on high voltage inverter retrofit for fans and pumps in power plants," in *Proc. CIGRE Sessions*, 2012, pp. 26–31.

[8] M. Tilscher, B. Lauter, and J. Lindenmaier, "Superimposing planetary gears as variable speed drives for rotating equipment," in *Proc. Asia Turbomachinery Pump Symp. Turbomach. Lab.*, 2018, pp. 1–5.

[9] T. Szolc, R. Konowrocki, M. Michajáow, and A. Prágowska, "An investigation of the dynamic electromechanical coupling effects in machine drive systems driven by asynchronous motors," *Mech. Syst. Signal Process.*, vol. 49, nos. 1–2, pp. 118–134, Dec. 2014.

[10] M. T. Khabou, N. Bouchaala, F. Chaari, T. Fakhfakh, and M. Haddar, "Study of a spur gear dynamic behavior in transient regime," *Mech. Syst. Signal Process.*, vol. 25, no. 8, pp. 3089–3101, Nov. 2011.

[11] W. Bai, D. Qin, Y. Wang, and T. C. Lim, "Dynamic characteristics of motor-gear system under load saltations and voltage transients," *Mech. Syst. Signal Process.*, vol. 100, pp. 1–16, Feb. 2018.

[12] S. Bai and S. Caro, *A Nonlinear Motor-Gear Model and its Application to Share-loading Analysis of Wind Turbine Yawing Mechanisms*. London, U.K.: Oxford Univ. Press, 2011.

[13] Y. Yi, D. Qin, and C. Liu, "Investigation of electromechanical coupling vibration characteristics of an electric drive multistage gear system," *Mech. Mach. Theory*, vol. 121, pp. 446–459, Mar. 2018.

[14] W. Bai, D. Qin, Y. Wang, and T. C. Lim, "Dynamic characteristic of electromechanical coupling effects in motor-gear system," *J. Sound Vib.*, vol. 423, pp. 50–64, Jun. 2018.

[15] C. Liu, X. Yin, Y. Liao, Y. Yi, and D. Qin, "Hybrid dynamic modeling and analysis of the electric vehicle planetary gear system," *Mech. Mach. Theory*, vol. 150, Aug. 2020, Art. no. 103860.
[16] R. Shu, J. Wei, R. Tan, X. Wu, and B. Fu, "Investigation of dynamic and synchronization properties of a multi-motor driving system: Theoretical analysis and experiment," *Mech. Syst. Signal Process.*, vol. 153, May 2021, Art. no. 107496.
[17] J. Song-Manguelle, S. Schroder, T. Geyer, G. Ekemb, and J.-M. Nyobe-Yome, "Prediction of mechanical shaft failures due to pulsating torques of variable-frequency drives," *IEEE Trans. Ind. Appl.*, vol. 46, no. 5, pp. 1979–1988, Sep. 2010.
[18] T. Feese and R. Maxfield, "Torsional vibration problem with motor/ID fan system due to PWM variable frequency drive," in *Proc. 37th Turbomach. Symp.*, 2008, pp. 1–10.
[19] J.-I. Itoh, N. Nomura, and H. Ohsawa, "A comparison between V/f control and position-sensorless vector control for the permanent magnet synchronous motor," in *Proc. Power Convers. Conf.-Osaka*, 2002, pp. 1310–1315.
[20] O. A. Lysenko and A. V. Simakov, "The pump hydraulic load effect determination on the parameters of an frequency-controlled asynchronous electric drive," in *Proc. Dyn. Syst., Mech. Mach.*, 2019, pp. 1–16.
[21] X. Han and A. B. Palazzolo, "VFD machinery vibration fatigue life and multi-level inverter effect," in *Proc. IEEE Ind. Appl. Soc. Annu. Meeting*, Oct. 2012, pp. 1–15.
[22] J. Song-Manguelle, G. Ekemb, D. L. Mon-Nzongo, T. Jin, and M. L. Doumbia, "A theoretical analysis of pulsating torque components in AC machines with variable frequency drives and dynamic mechanical loads," *IEEE Trans. Ind. Electron.*, vol. 65, no. 12, pp. 9311–9324, Dec. 2018.
[23] L. Zhang, Q. Wu, Z. Ma, and X. Wang, "Transient vibration analysis of unit-plant structure for hydropower station in sudden load increasing process," *Mech. Syst. Signal Process.*, vol. 120, pp. 486–504, Apr. 2019.
[24] C. Mao, J. Ding, and Y. Gan, "A novel fast speed regulation control strategy for VVVF in HVF," in *Proc. Asia–Pacific Power Energy Eng. Conf.*, Mar. 2009, pp. 1–5.
[25] B. Bilgin, J. Liang, M. Terzic, and J. Dong, "Modeling and analysis of electric motors: State-of-the-art review," *IEEE Trans. Transport. Electrific.*, vol. 5, no. 3, pp. 602–617, Sep. 2019.
[26] A. Diaz, R. Saltares, C. Rodriguez, R. F. Nunez, E. I. Ortiz-Rivera, and J. Gonzalez-Llorente, "Induction motor equivalent circuit for dynamic simulation," in *Proc. IEEE Int. Electric Mach. Drives Conf.*, May 2009, pp. 858–863.
[27] T. Bhattacharjee, M. Jamil, and A. Jana, "Design of SPWM based three phase inverter model," in *Proc. Technol. Smart-City Energy Secur. Power (ICSESP)*, Mar. 2018, pp. 1–6.
[28] B. Gou, Y. Xu, Y. Xia, Q. Deng, and X. Ge, "An online data-driven method for simultaneous diagnosis of igbt and current sensor fault of three-phase PWM inverter in induction motor drives," *IEEE Trans. Power Electron.*, vol. 35, no. 12, pp. 13281–13294, Dec. 2020.

DIANRUI WANG received the B.S. degree from the School of Mechanical Engineering, Taiyuan University of Technology, Taiyuan, Shanxi, in 2019. He is currently pursuing the M.S. degree in mechanical engineering with Shandong University, Jinan, Shandong.

His research interests include the electromechanical dynamic, precision drive, and transmission.

FUCHUN YANG received the B.S. degree from the School of Mechanical and Energy Engineering, Zhejiang University, Hangzhou, Zhejiang, China, in 2004, and the Ph.D. degree in mechanical engineering from Zhejiang University, in 2009.

From 2014 to 2015, he was a Visiting Scholar at Virginia Tech. He is currently an Associate Professor with Shandong University. His research interests include mechanical dynamics, precision drive, and transmission and robots.

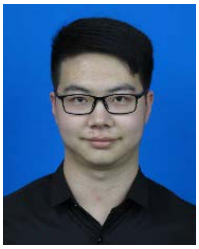

XIAOFENG JIANG received the B.S. degree from the School of Mechanical Engineering, Shandong University, Jinan, Shandong, in 2020, where he is currently pursuing the M.S. degree in mechanical engineering.

His research interests include precision drive and transmission and robots. In the 2020–2021 academic year, he won the postgraduate freshman scholarship, and in the 20021–2022 academic year, he won the second-class continuation scholarship for postgraduates.

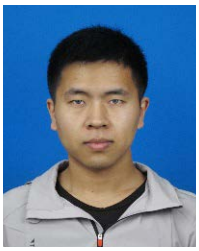

SHUAI SHI received the B.S. degree from the School of Mechanical Engineering, Shandong University, Jinan, China, in 2020, where he is currently pursuing the M.S. degree in mechanical engineering with the School of Mechanical Engineering.

His research interests include the electromechanical systems and robots.

SONGHUA MA received the B.S. degree from the School of Mechanical Engineering, Shandong University, Jinan, Shandong, in 2008, and the Ph.D. degree in mechanical engineering from Tsinghua University, Beijing, China, in 2014.

She is currently an Associate Researcher with Shandong University. Her research interests include CAD/CAM, modern design theory, knowledge engineering, engineering change management, and enterprise informatization.